

Alma Mater Studiorum Università di Bologna
Archivio istituzionale della ricerca

Nanostructured Co₃O₄ electrocatalyst for OER: The role of organic polyelectrolytes as soft templates

This is the final peer-reviewed author's accepted manuscript (postprint) of the following publication:

Published Version:

Bhatti A.L., Tahira A., Gradone A., Mazzaro R., Morandi V., Aftab U., et al. (2021). Nanostructured Co₃O₄ electrocatalyst for OER: The role of organic polyelectrolytes as soft templates. ELECTROCHIMICA ACTA, 398, 1-11 [10.1016/j.electacta.2021.139338].

Availability:

This version is available at: <https://hdl.handle.net/11585/879492> since: 2023-04-28

Published:

DOI: <http://doi.org/10.1016/j.electacta.2021.139338>

Terms of use:

Some rights reserved. The terms and conditions for the reuse of this version of the manuscript are specified in the publishing policy. For all terms of use and more information see the publisher's website.

This item was downloaded from IRIS Università di Bologna (<https://cris.unibo.it/>).
When citing, please refer to the published version.

(Article begins on next page)

This is the final peer-reviewed accepted manuscript of:

Adeel Liaquat Bhatti, Aneela Tahira, Alessandro Gradone, Raffaello Mazzaro, Vittorio Morandi, Umair Aftab, Muhammad Ishaq Abro, Ayman Nafady, Kezhen Qi, Antonia Infantes-Molina, Alberto Vomiero, Zafar Hussain Ibupoto, *Nanostructured Co₃O₄ electrocatalyst for OER: The role of organic polyelectrolytes as soft templates*, Electrochimica Acta, Volume 398, 2021, 139338.

The final published version is available online at:
<https://doi.org/10.1016/j.electacta.2021.139338>

Terms of use:

Some rights reserved. The terms and conditions for the reuse of this version of the manuscript are specified in the publishing policy. For all terms of use and more information see the publisher's website.

This item was downloaded from IRIS Università di Bologna (<https://cris.unibo.it/>)

When citing, please refer to the published version.

Nanostructured Co₃O₄ electrocatalyst for OER: the role of organic polyelectrolytes as soft templates

Adeel Liaquat Bhatti^a, Aneela Tahira^b, Alessandro Gradone^{d,j}, Raffaello Mazzaro^{d*}, Vittorio Morandi^d, Umair aftar^c, Muhammad Ishaq Abro^c, Ayman Nafady^h, Kezhen Qi^g, Antonia Infantes-Molinaⁱ, Alberto Vomiero^{e,f}, Zafar Hussain Ibupoto^{b*}

^aInstitute of Physics University of Sindh Jamshoro, 76080, Sindh Pakistan

^bDr. M.A Kazi Institute of Chemistry University of Sindh Jamshoro, 76080, Sindh Pakistan

^cDepartment of Metallurgy and Materials Engineering, Mehran University of Engineering and Technology, 7680 Jamshoro, Sindh Pakistan

^dInstitute for Microelectronics and Microsystems, Italian National Research Council, Section of Bologna, Via Piero Gobetti 101, 40129, Bologna, Italy

^eDivision of Material Science, Department of Engineering Sciences and Mathematics, Luleå University of Technology, 97187 Luleå, Sweden

^fDepartment of Molecular Sciences and Nanosystems, Ca' Foscari University of Venice, Via Torino 155, 30172 Venezia Mestre, Italy

^gInstitute of Catalysis for Energy and Environment, College of Chemistry and Chemical Engineering, Shenyang Normal University, Shenyang 110034, China

^hDepartment of Chemistry, College of Science, King Saud University, Riyadh 11451, Saudi Arabia

ⁱDepartment of Inorganic Chemistry, Crystallography and Mineralogy. (Unidad Asociada al ICP-CSIC), Faculty of Sciences, University of Malaga, Campus de Teatinos, 29071 Malaga, Spain.

^jDepartment of Chemistry "G.Ciamician", University of Bologna, Via Selmi 2, 40126, Bologna, Italy.

Corresponding authors: Zafar Hussain Ibupoto, PhD*, Raffaello Mazzaro, PhD

Email address: zaffar.ibhupoto@usindh.edu.pk, mazzaro@bo.imm.cnr.it

Abstract

Designing an efficient electrocatalyst for the oxygen evolution reaction (OER) in alkaline media is highly needed but very challenging task. Herein, we used organic polyelectrolytes (carboxymethyl cellulose) CMC and polyacrylamide polymers for the growth of Co_3O_4 nanostructures by aqueous chemical growth method. The morphology and composition studies were performed on scanning electron microscopy (SEM), energy dispersive X-ray (EDX), powder X-ray diffraction (XRD), X-ray photoelectron spectroscopy (XPS) and high-resolution transmission electron microscopy (HRTEM) techniques. The structural properties and the surface chemistry of the metal oxide electrocatalysts were correlated to the OER performance, and the enhancement mechanism with respect to pristine Co_3O_4 was observed to be specifically related to the polyelectrolyte templating role.

Co_3O_4 @CMC composites displayed reduced crystallite size, producing OER overpotential as low as 290 mV at 10 mAcm^{-2} in 1.0 KOH and Tafel slope of 71 mVdec^{-1} , suggesting fast transfer of intermediates and electrons during water electrolysis. On the other hand, the use of polyacrylamide and its different templating mechanism resulted in similar crystallite size, but preferential exposed faces and larger surface vacancies content, as demonstrated by HR-TEM and XPS, respectively. Consistently, this material displays cutting-edge OER performance, such as overpotential equal to 260 mV at 10 mAcm^{-2} and a low Tafel slope of 63 mVdec^{-1} . The proposed strategy for the preparation of Co_3O_4 nanostructures in the presence of CMC and polyacrylamide is facile, mass production, could equally contributed towards the realization of hydrogen energy. Therefore, these nanostructures of Co_3O_4 can be regarded as an alternative and promising materials for the different electrochemical applications including fuel cells, metal air batteries, overall water electrolysis and other energy storage devices.

Keywords. Polyacrylamide, carboxymethyl cellulose, Co_3O_4 , oxygen evolution reaction, alkaline media

1. Introduction

Since several decades, there is a drastic increase in the energy demands as our activities in daily life are mainly supported by the availability of energy. The international energy agency has reported an increase of 2.3% of energy demand in 2018. This rise in energy demand is double to that of last decade [1]. Most of the energy (approximately 70%) is coming from the fossil fuels. By the end of 2040, the energy demands will cross by 40% as described in the future- outlook of energy in 2018. The continuous use of fossil fuels is not only increasing their cost, but it also shows adverse effect on our environmental conditions due to the emission of greenhouse gases. Nature is also associated with wide range of alternative energy resources including wind, solar, ocean, water, bioenergy, geothermal, etc. [2]. Water splitting is a potential energy resource for reducing the impact of non-renewable energy resources, and it can also reduce the impact of carbon contamination, as this technology produces green fuels with zero carbon emission [3]. Water splitting involves two processes namely oxygen evolution reaction (OER), and hydrogen evolution reaction (HER). The complete dissociation of water produces H_2 and O_2 via HER at the cathode electrode and OER at the anode electrode respectively [4]. Electrocatalysis is a promising technology for increasing the energy resources through the consumption of water and electricity [5]. Electrocatalysis shows that two processes (HER/OER) have different kinetics as HER involves a two-electron transfer process [6], whereas OER is four electrons transfer process [7]. Therefore, OER is complicated and kinetically slow, thus requiring efficient catalysts. For this reason, there is a need to design efficient electrocatalysts with high density of catalytic sites to lower the overpotential for the OER process [8,9]. Several catalysts including Ir/Ru based materials are extensively used for the OER, but their large-scale use creates economic stress and also their rare abundance is another limitation for scalable processes. Furthermore, transition metal oxides are found promising materials for OER applications as they are abundant and low cost. The oxides of Fe, Ni, Co, and Cu are widely studied for OER due to their rich active sites for catalysis [10-15]. However, these materials have high overpotential, poor stability and durability in alkaline media. To shape the successful overall water splitting for practical applications, efficient OER catalysts must be developed. For this purpose, different earth-abundant cobalt-based catalysts particularly cobalt oxide (Co_3O_4) materials are performing very well [16-18]. However, the Co_3O_4 is easy to restack and is associated with poor conductivity, which further limits its OER activity, and shows kinetically slow OER kinetics[16].

Co₃O₄ growth can be templated by various small molecules, producing a wide set of different morphologies, and influencing the electrochemical activity [19, 20, 21, 22]. The same approach has not been experienced with polymeric sacrificial templates, providing both many functional groups and mechanical constraints resulting from the backbone chain. In this study, we investigate the role of two different polymers as soft surface template for the hydrothermal growth of Co₃O₄ nanostructures, namely polyacrylamide and sodium carboxymethyl cellulose.

These polymers are both displaying nucleophilic functional groups and, in the reaction conditions, a large number of negative charges due to the presence of carboxylate groups, expected to **complex** the cobalt salt during the cobalt hydroxide precipitation [23], as well as to stabilize the growing nanocrystals.

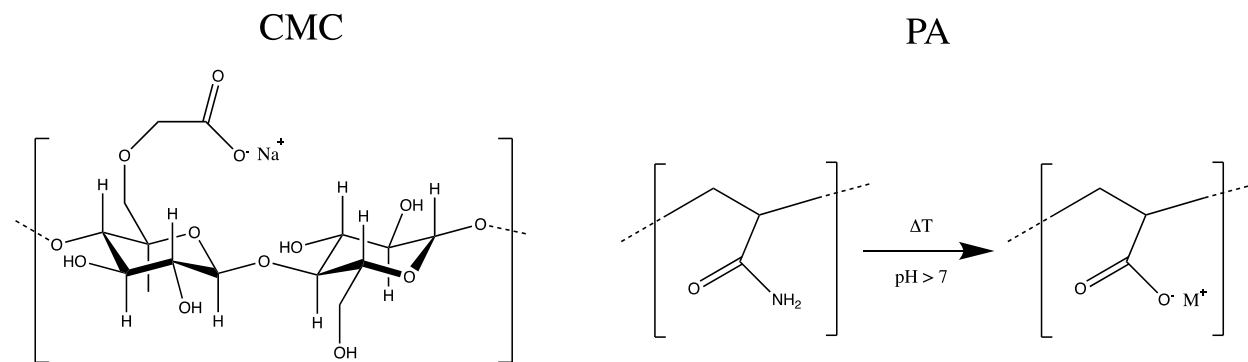


Figure 1. Schematic representation of carboxymethyl cellulose and polyacrylamide structure, and the hydrolysis mechanism of the latter.

Carboxymethyl cellulose (CMC) is a common cellulose derivative obtained by cellulose reaction with chloroacetic acid. The resulting carboxylic acid derivatives are deprotonated due to the basic environment and the obtained material is generally distributed as sodium salt. CMC is widely employed as a thickener or viscosity modifier [24] due to the possibility to tune the hydrophilic character and the resulting rheological properties by controlling the degree of substitution of pristine cellulose. The tunable hydrophilicity of CMC is also employed to stabilize multiple suspensions [25] in industrial applications. Additionally, CMC is inexpensive, chemically stable and highly suitable for mass production of composite materials. There are several examples of CMC based hydrogels integrating metal oxides [26] and few examples of metal oxides growth templated by CMC microspheres [27] but the role of the polyelectrolyte during hydrothermal synthesis process was not investigated, to the best of our knowledge. CMC is also known to spontaneously produce nanofibers

that might influence the metal oxide growth process and the resulting porosity, enhancing the performance of electrochemical reactions [28].

Polyacrylamide (PA) is a hydrophilic polymer resulting from the homo-polymerization of acrylamide. The hydrophilicity is driven by the large number of amide functional groups, whose slightly nucleophilic character is known to stabilize electrophilic metal derivatives [29]. Polyacrylamide is also known to spontaneously decompose at elevated temperature or pH [30] due to the hydrolysis of the amide group and the resulting formation of a carboxylic acid and ammonia. The hydrolyzed polymer becomes a temperature-induced polyelectrolyte with either anionic or cationic character [31] depending on the reaction conditions. PA, in its anionic form, is widely employed as stationary phase in gel electrophoresis. In addition, thanks to the large number of negative charges, it is widely employed in wastewater treatment to flocculate insoluble particles and metal precipitation [32]. A recent study shows that polyacrylamide microspheres exhibit metallophilic properties which significantly carried precursor salt with the homogenous distribution [33].

In this study, we used a polyacrylamide/CMC as soft surface template for the deposition of cobalt oxide (Co_3O_4) nanostructures. Unlike previous reports of hydrothermal growth methods for Co_3O_4 nanostructures employing small molecular templates, the use of polymeric templates with multiple functional charged groups is expected to direct the metal oxide growth and efficiently stabilize the growing structure. The use of these organic polyelectrolytes (PA is acting as one in the hydrothermal conditions employed) allows for a cheap and robust preparation process of a functional materials with robust OER activity, which fosters the OER kinetics.

Herein, the role of these two polymers, CMC and polyacrylamide, will be investigated with respect to their ability to act as soft templates for Co_3O_4 growth. The resulting morphology and structure are thoroughly investigated, and the material is eventually evaluated as electrocatalyst for OER. The Co_3O_4 nanostructures grown in the presence of CMC display a low overpotential of 290 mV at 10 mA cm^{-2} and a small Tafel slope of 71 mV dec^{-1} , whereas the use of polyacrylamide resulted even lower Tafel slope and overpotential of 63 mV dec^{-1} and 260 mV respectively. The improved electrochemical performance was correlated with the modified nanoscale morphology, thoroughly investigated by electron microscopy and x-ray diffraction analysis.

2. Materials and Methods

2.1.Synthesis of Co₃O₄ nanostructures

Polyacrylamide, (carboxymethyl cellulose) CMC, urea, cobalt chloride hexahydrate, potassium hydroxide, 20% RuO₂/C and absolute ethanol were obtained from Sigma Aldrich Karachi, Pakistan. All the solutions were prepared in the deionized water. For the synthesis of cobalt oxide nanostructures using nucleophilic CMC/polyacrylamide polymers, the following methodology was used: An equimolar solution (0.1M) of cobalt chloride hexahydrate and urea was prepared in two separate beakers with a volume of 100 mL. In each beaker, an amount of 25, and 50mg of CMC was added and they were named as Co₃O₄@CMC-1 (S1), and Co₃O₄@CMC-2 (S2). Similarly, 25, and 50 mg of polyacrylamide were added in two separate beakers along with cobalt chloride precursor and they were labeled as Co-25polyacryl and Co-50polyacryl, respectively. Then homogenous solutions were obtained by the mechanical stirring for 30 min. The growth solutions were covered with an aluminum sheet to prevent the evaporation of solvent molecules. Afterward, the growth solutions were kept in an oven for 6 h at 90 °C. Afterwards, the samples were filtered on the laboratory filter paper and the pinkish filtrate cobalt hydroxide powder was collected. This powder was finally annealed at 500 °C for 5 hs in air to transform hydroxide product into oxide phase. The pristine Co₃O₄ was also prepared by the same growth technique.

2.2.The structural, and compositional characterization

The investigations about structure and morphology were done with SEM and XRD techniques. The XRD measurement was performed at CuK α radiation ($\lambda = 1.5418 \text{ \AA}$), 45 kV and 45 mA. The SEM was carried out at 3 Kv. The structure and composition analysis in the nanoscale were carried out with a FEI Tecnai F20 high resolution transmission electron microscope (HR-TEM) operated at 200 kV, equipped high angle annular dark field scanning transmission electron microscopy (HAADF – STEM) detector and an energy dispersive spectrometer (EDS) for the determination of the chemical composition. The-ray photoelectron spectra (XPS) were collected using a Physical Electronics PHI 5700 spectrometer with non-monochromatic Al K α radiation (300W, 15 kV, 1486.6 eV) for the analysis of the core level signals of C 1s, O 1s, Co 2p and CoLMN and with a multi-channel detector. Binding energy (BE) values were referenced to the C 1s peak (284.8 eV) from the adventitious contamination layer. The PHI ACCESS ESCA-V6.0 F software package and Multipak v8.2b were used for acquisition and data analysis, respectively. A Shirley-type background was subtracted from

the signals. Recorded spectra were always fitted using Gauss-Lorentz curves, in order to determine the binding energy of the different element core levels more accurately. The error in BE was estimated to be *ca.* 0.1 eV.

2.3. The oxygen evolution reaction characterization of Co₃O₄ in alkaline media

The electrochemical experiments were performed with cyclic voltammetry (CV), linear sweep voltammetry (LSV), chronopotentiometry, and EIS. Prior to these electrochemical modes, glassy carbon (GC) electrode wetted with alumina slurry of (0.5 μm) and polished by the silicon paper. Then GC electrode was washed with the deionized water. Different catalyst materials with a mass of 5 mg were dissolved in the deionized water and 50 μL of 5% of Nafion as a binder was also added. A uniform catalyst ink was obtained by the sonication. Then GC electrode was modified with 5 μL (0.2 mg) of the catalyst ink. Afterwards, the modified GC electrode was dried at room temperature. The electrochemical experiments were performed with three electrodes configuration. The reference electrode was silver-silver chloride (Ag/AgCl) and it was filled with 3M KCl, counter electrode was graphite rod, and the working electrode was modified GC. The cyclic voltammetry was used at 10 mV/s to ensure the stability of working electrode, then electrochemical tests in a 1.0M aqueous solution of KOH of pH 13 were measured. The durability of two best Co₃O₄ samples was studied by the chronopotentiometry at a constant 15 mA/cm² and 10 mA/cm². The experimental conditions for the EIS were 100 kHz to 0.1 Hz with a sinusoidal potential of 10 mV and OER onset potential 1.46 V vs RHE. The onset potential was estimated from the tangents in non-faradaic region i.e horizontal line and faradaic region of LSV curve. The abscissa of intersection of these points is giving the value of onset potential. All the electrochemical studies were performed at standard conditions. The potentials of Ag/AgCl were covered into reversible hydrogen electrode (RHE) using Nernst equation.

3. Results and discussion

3.1. The physical characterization of nanostructured Co₃O₄ material

SEM micrographs of the samples are displayed Figure 1. All samples are characterized by complex nanostructures. Pristine Co₃O₄ exhibit quasi-spherical nanoparticles aggregated into platelets-like structures. The platelets exhibit a length of few microns and diameter of 200-500 nm Figure 1a. The Co₃O₄@CMC-1 exhibit more irregular character, with elongated nanowire-like structures composed

by nanoparticles, as shown in Figure 1b. The elongated character is highlighted upon increasing the CMC content (Figure 1c), displaying highly oriented nanowires resulting from the linear self-assembly of nanoparticles. The length of these nanowires of 2-3 microns and an average diameter of 100-150 nm. Polyacrylamide addition results in a progressive loss of the flower-like orientation of nanowires, which is completely lost upon adding 50mg of polyacrylamide in the reaction batch Figure 1 d,e. The composite structure is still consisting a self-assembly of nanoparticles, but their shape is now elongated and regular. The change in morphology might be resulting from the templating effect of the polyacrylamide during the growth process, thanks to the slightly basic amide group. The composition of the sample was confirmed by EDS analysis, obtaining only Co and O signal, in addition of a spurious Sn-related peak coming from the analysis substrate (Fig. S1).

Structural analysis is performed by powder XRD on all the prepared samples, including bare Co_3O_4 , and it is reported in figure 2. All samples exhibit a clear crystalline diffractogram, whose peaks can be indexed as face centered cubic Co_3O_4 phase, reference card no. (96-900-5896). The sharp reflection peaks pointing the excellent crystalline properties of the materials. The XRD study ensures the high degree of purity and single-phase system for the prepared Co_3O_4 samples, with no residual of additional phase resulting from the polymer addition. No specific variation of the observed crystalline phase is observed, as expected. Interestingly, all the Co-polyacryl samples exhibit increased 004/113 peaks ratio, suggesting a preferential growth axis.

Figure 3 is displaying low and high magnification HR-TEM micrographs for Co_3O_4 (a,b,c), Co-25polyacryl (d,e,f) and Co_3O_4 @CMC-2 g,h,i) samples, in order to compare the role of template during the growth process on nanoscale structure and morphology. As suggested by SEM analysis, pristine Co_3O_4 sample and Co_3O_4 @CMC-2 exhibit spherical-shape nanocrystallites while Co-25polyacryl displays nanoparticles with a rounded parallelepiped geometry.

The high magnification micrographs of all samples confirm the crystalline character of the material, with crystal phase compatible with the one of Co_3O_4 with a spinel like structure (Figure 3c,f,i). In particular, it is possible to notice that the presence of polyacrylamide affects the shape of the nanoparticles, moving from a more random, almost spherical shape of the pristine sample (figure 3a,b) and the CMC-templated sample (figure 3g,h) to a more rectangular one for the case with polyacrylamide (Figure 3d,e). By comparing the diffraction fringes pattern on HR-TEM micrograph

of a single Co_3O_4 crystal (Fig. 3f) with the one of a Co-25polyacryl crystal (Figure 3e), it is possible to notice a set of lattice planes parallel to the crystal squared edge, with d-spacing equal to 0.28 nm (FFT in the inset). These planes can be indexed as the (1,-1,0) planes, and may represent one of preferentially exposed faces of the nanocrystal, given his squared shape. The edge perpendicular to the (1,-1,0) planes does not display any parallel planes on the specific zone axis, while we can observe two sets of planes with 0.24 nm d-spacing, relative to the planes orthogonal to the (1,3,-1) and (3,1,-1) directions, whose direction is equally tilted with respect to the edge direction. While no specific set of planes can be visualized on the perpendicular edge, this may be resulting from a slight tilting of the nanocrystal on the (1,-1,0) axis and the squared edge might be resulting from (1,1,1) planes, which are often observed to be perpendicular to nanocrystals squared edges, with the relative d-spacing equal to 0.46 nm. This behavior is observed in multiple nanocrystals (figure S2), suggesting that (1,-1,0) and (1,1,1) planes may be the nanocrystals preferential exposed faces due to a selective polyacrylamide templating effect. Due to the limited size of the nanocrystals and the inhomogeneous size ratio, we expect that this morphology-related singularity of polyacrylamide-templated Co_3O_4 to be hardly detected by XRD analysis.

This specificity of polyacrylamide templated Co_3O_4 may result in a different electrochemical activity resulting from the different activity of the exposed crystal faces and the resulting surface chemistry. However, a deeper structural investigation is needed to assess the role of this peculiar morphology with respect to the functional properties, addressing the 3D morphology of the nanocrystals.

The size distribution of the nanocrystals was extracted from the low magnification HR-TEM micrographs and reported in Figure S3, to understand the average dimension of the nanoparticles and the possible variation due to the templating agents. Figure S3a and S3b shows that the size of the crystalline domains (measured either as the diameter or the diagonal if the geometry is closer to spherical or squared, respectively) does not change moving from the pristine Co_3O_4 to the Co-25polyacryl, with an average value approaching 60 nm. On the opposite, lower average particle size can be noticed for Co_3O_4 @CMC-2 sample (Figure S3c), dropping to 44.4 nm (with a comparable standard deviation), suggesting that the cellulose-based polyelectrolyte enhances the nucleation step and limits the crystallite growth maximum size during the hydrothermal synthesis process.

STEM-EDS analysis of the polyacrylamide-treated Co_3O_4 sample confirms the presence of cobalt and oxygen with the addition of a peak relative to the Cl (Figure S4). In all the highlighted spot (orange circles) the ratio in atomic percentage between Co and O does not change (value in average $\text{Co/O} = 0.62$), suggesting homogeneous composition (Figure S4a). In case of Cl, the atomic percentage is very low (around 1%) but it increases if focusing onto the areas with lower contrast (spot 1), with a value of 3% (Figure S4b). The reason for the presence of Cl can be traced back to residuals of the counter-ion employed during preparation. In addition, the presence of chlorine may be the reason for the presence of porous or otherwise thinner areas.

EDS profile of the sample $\text{Co}_3\text{O}_4@\text{CMC-2}$ (Figure S5) is displaying the same behavior observed in the previous case, with a Co/O content ratio constant for all the profile reconstruction (Figure S4b). The evaluation of the atomic percentage of the different chemical components further confirms the crystal phase analysis, with an average ratio Co/O of 0.65.

The chemical state and surface composition of the Co-25polyacryl and Co_3O_4 CMC-2 based samples and the pristine Co_3O_4 were evaluated by X-ray photoelectron spectra (XPS) technique. Co $2p$, Co_{LMN} and O $1s$ core level spectra are included in Figure 4.

Cobalt photoelectron signal (Figure 4a) shows the characteristic peaks of Co $2p_{3/2}$ (Solid lines) and Co $2p_{1/2}$ (Dotted lines) doublet. All the three samples show the characteristic spectrum of cobalt spinel phase and the decomposition of the spectra was carried out by following the indications reported by Biesinger et al.[34]. Focusing on the Co $2p_{3/2}$ component, several contributions are present. According to the literature [35], the peak at ca. 779.5 eV corresponds to Co^{3+} , the peak at 780.9 eV to Co^{2+} , and the signal at 782.5 eV to Co^{2+} in $\text{Co}(\text{OH})_2$. For the fitting, also the two shake-up satellites (surface and bulk plasmons) of cobalt ions were included [36]. The decomposition results are summed up in Table 1. It was worth noting that the binding energy of Co $2p$ hardly changed between the samples.

Further insights about the chemical state of cobalt was obtained from the Co_{LMN} Auger signal, being more sensitive to chemical state modifications of cobalt. The corresponding spectra in terms of kinetic energy (KE) of Co_{LMN} electrons are depicted in Figure 4b. Three peaks are observed at about 774.5, 770.0 and 766.2 eV corroborating the presence of three main species of cobalt. From these signals, the corresponding modified Auger parameter (α') was determined to perform a tentative assignment of these components. It was calculated according to the following equation:

$$\alpha' = 1486.6 + KE_{Co_{LMN}} - KE_{Co2p}$$

where KE (Co_{LMN}) is the kinetic energy of the Co_{LMN} Auger electron, KE Co 2p is the kinetic energy of the Co 2p_{3/2} photoelectron and 1486.6 is the energy of the Al K α X-ray excitation in eV. The obtained values were three sets of points, the first one located at ca. 1554.2 eV in the region of Co³⁺; the second one at 1550.9 eV, in the Co²⁺ region; and a third one at 1549.0 eV corresponding to the region of Co(OH)₂ species. These data corroborate those obtained from the photoelectron signal analysis.

The quantification of the spectra provided the following Co³⁺/Co²⁺ surface atomic ratios were 0.90, 1.07 and 0.96 for the Co₃O₄, Co-25polyacryl and Co₃O₄@CMC-2, respectively, indicating that Co-25polyacryl possessed relatively more Co³⁺ ions on the surface than the other samples.

Considering O 1s signal (Figure 4c) for each sample, the spectra decomposition provides three peaks contributions: the main one with a binding energy at ~529.9 eV and assigned to surface lattice oxygen species (denoted as O_{Lat}) on cobalt spinel [37], the second contribution with binding energy at ~531.2 eV was ascribed to low coordination oxygen species (O₂, O₂²⁻ and O⁻) or surface oxygen species adsorbed over the surface oxygen vacancy (denoted as O_{Surf}) [38] and the binding energy around at ~533.0 eV is reported in the literature to be due to chemisorbed oxygen (represented as O_{Che}), respectively [39]. O_{Surf} has greater mobility than lattice oxygen and may give rise to beneficial spillover phenomena at the solid surface [40]. Quantitative analyses of the decomposed O 1s XPS spectra provided the O_{Surf}/O_{Lat} ratios on the surface and summarized in Table X. It revealed that the Co-25polyacryl showed the highest O_{Surf}/O_{Lat} atomic ratio, followed by Co₃O₄@CMC-2 and Co₃O₄, and therefore indicating that Co-25polyacryl has more surface oxygen vacancies that could provide enough oxygen adsorption sites or active centers for the process as found in literature [41]. Moreover, it has been reported that the higher the O_{Surf}/O_{Lat} atomic ratio the lower the energy to activate molecules into reactive oxygen species [42]. Previous XPS studies [43] has been proven that the abundance of surface Co³⁺ species on the surface can be conducive to the transport of the oxygen species with a higher efficiency [44]. The above-mentioned results revealed that Co-25polyacryl with more surface Co³⁺ and based on the principle of electro-neutrality, the atomic ratio of O_{Surf}/O_{Lat} is also the highest, implies that this sample with a larger amount of surface oxygen vacancies, the enhancement of Co³⁺ concentration can impact in oxygen desorption. We infer that the rise of preferential exposed faces in the more regular, rounded parallelepiped morphology, exhibited by Co-polyacryl samples, might be

related to the higher amount of oxygen vacancies, whose increase might be resulting from the polyacrylamide hydrolysis and surface cobalt coordination process. The polyacrylamide addition is therefore affecting the metal oxide growth through a complex, multistep impact, unlike what observed with the addition of a less unpredictable polyelectrolyte such as CMC, expected to exert merely a colloidal stabilization effect on the growing nanocrystals due to the multiple carboxylate groups.

3.2. The oxygen evolution reaction activity of nanostructured Co₃O₄

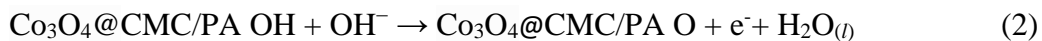
The functionality of as prepared pristine Co₃O₄, Co-25polyacryl, Co-50polyacryl, Co₃O₄@CMC-1 and Co₃O₄@CMC-2 materials was investigated using a cell set up of three electrodes in 1.0M KOH. First, a slow CV at 10 mV/s was performed to limit the capacitive current and corresponding polarization curves were measured. Figure 5a shows the LSV polarization curves for Co₃O₄@CMC-2, Co₃O₄@CMC-1, and pristine Co₃O₄ with an onset potential of 1.48, 1.50 and 1.63 V, versus RHE respectively. The Co₃O₄@CMC2 has the lowest onset potential and an excellent OER activity. The calculated overpotential for the Co₃O₄@CMC-2 is 290 mV at 10 mAcm⁻². Co₃O₄@CMC-1 sample exhibits an overpotential of 300 mV which is still better than the pristine Co₃O₄. The extremely low overpotential value attained by Co₃O₄@CMC-2 strongly improves the state of the art with respect to similar Co based electrocatalysts and other materials for OER. [45-49]. This improvement might be related to the reduce particle size achieved by employing CMC as soft template. The best performance for Co₃O₄@CMC samples is coming from the highest loading of CMC during the synthesis process, suggesting that some improvement might be achieved with even higher loading.

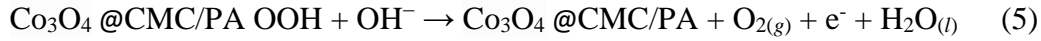
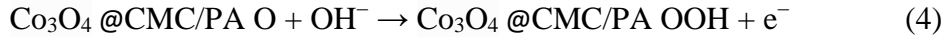
Figure 5e displays LSV polarization curves for Co-25polyacryl and Co-50polyacryl samples, together with RuO₂/C, used as a high-performance OER electrocatalysis reference material. The calculated overpotentials at 10 mAcm⁻² are 260, 300 and 160 mV for the Co-25polyacryl, Co-50polyacryl and RuO₂/C, respectively. Being a noble material RuO₂ has shown excellent performance as expected, however the development for the design of efficient nonprecious material for OER is a prime need, and a Co-based catalysis with comparable performance would be ideal. By comparing the results with pristine Co₃O₄ and CMC-templated one, we can notice a further improvement of the onset potential for the PA-templated Co₃O₄ samples, at low PA content. For comparison purpose, Co₃O₄ thin film obtained from wet chemical method display a much larger value equal to 377 mV at 10 mAcm⁻² [50]. Various phases of cobalt oxide, including CoO and Co₃O₄ were reported in the literature to produce

even higher overpotentials of 495 and 496 mV at 10 mA cm⁻², respectively [51]. mesoporous Co₃O₄ obtained by silica hard-templating approach was also reported with relatively high OER overpotential of 592 mV [52]. The further improvement of OER overpotential achieved by employing PA as soft template confirms the viability of the proposed approach. The structural and spectroscopical analysis suggested a different templating mechanism for polyacryl-assisted growth. The improved electrochemical performance is consistent with the larger O_{Surf}/O_{Lat} observed by XPS, but while the crystallite size is basically not affected by PA presence, the shape and the nanocrystals morphology are influenced by its addition. As a consequence, we may infer that the preferential exposed faces in the squared-shape crystallites are more active towards OER. Thus, PA addition could allow for improved active surface.

The OER activity could be further described from Tafel value [53,54], as shown in Figure 5b. The Tafel slope of Co₃O₄@CMC-2 composite was found 71 mVdec⁻¹ and observed lower than the Co₃O₄@CMC-1 (76mVdec⁻¹) and pristine Co₃O₄ (164 mVdec⁻¹). An even larger drop is experienced for the Co-25polyacryl, with an ultra-low value of 63 mV dec⁻¹, approaching the one of the reference noble metal catalyst RuO₂/C, equal to 55 mVdec⁻¹. Interestingly, upon increasing the PA content during the metal oxide growth process, the Tafel slope increases to 82mV dec⁻¹, suggesting a more degree of oxygen-containing reaction intermediates for the enhanced OER process. It is clear from LSV curves that an optimum level of polyacryl is essential to enhance the catalytic activity of Co₃O₄ and that further increase in the polymer concentration lowered the OER activity of Co₃O₄.

From LSV curves, we see the pre-oxidation peaks for the Co₃O₄ obtained with polyacrylamide and they are assigned to the oxidation of cobalt (II) to (III) [50]. Additionally, pre-oxidation peak is present in the RuO₂ sample due to the shift in oxidation from lower to higher oxidation state. It has been shown that OER mechanism is a four-electron process, which is not trivial. However, a general mechanism for OER in basic environment is discussed in several studies and stepwise processing is described below. It is believed that first Co³⁺ binds with OH⁻ as shown in steps 1 and 2. The CoOOH is produced with a continuous reaction of OH⁻ (step 3). Further, CoOOH adsorb additional OH⁻ and releases O₂ (step 4). It has been demonstrated that OER process transforms the Co₃O₄ into CoOOH as later is highly stable owing to higher oxidation state of cobalt [24].





Herein, $\text{Co}_3\text{O}_4 @\text{CMC/PA}$ is proposed as catalytic site for OER on the working electrode and step 3 is the rate governing step.

The durability of $\text{Co}_3\text{O}_4@\text{CMC-2}$ was studied through chronopotentiometry experiment at constant 15 mA/cm^2 as enclosed in Figure 5c and it was seen no rise in the potential during electrolysis, confirming it's an excellent stability. The superior OER activity was excellent stability makes the $\text{Co}_3\text{O}_4@\text{CMC-2}$ applicable for the wide range of applications. To reveal the stability of the $\text{Co}_3\text{O}_4@\text{CMC-2}$ material before and after the durability test, LSV curves were measured as shown in Figure 4d. The $\text{Co}_3\text{O}_4@\text{CMC-2}$ composite maintained the onset potential and current density without any drop and it confirms the good stability of our $\text{Co}_3\text{O}_4@\text{CMC-2}$ electrocatalyst.

Similarly, the polarization curves of Co_3O_4 with polyacrylamide Co-25polyacryl after durability experiment for 30 h were measured Figure 5 g. The activity of electrocatalyst remained constant without any change in the onset potential and current density. In addition, we investigated the durability of Co-25polyacryl via chronopotentiometry at constant current density of 10 mA cm^{-2} (Figure 5h). The potential was found to be constant for 30 h. The OER activity of as synthesized Co_3O_4 nanostructures with polyacrylamide was compared with already existing excellent OER electrocatalysts in terms of overpotential and Tafel slope is collected in Table S1. The performance of Co_3O_4 obtained with polyacrylamide as soft template is equal or superior to many of the reported OER catalysts, in terms of low overpotential and Tafel value. Both TEM and SEM studies are revealing that the morphology and enhanced surface area are the main factors which boosted the OER activity of $\text{Co}_3\text{O}_4@\text{CMC-2}$ and Co-25polyacryl. This could be attributed from the well orientation of nanowires which further enhanced the charge transfer kinetics and accelerated the OER process.

3.3. The electrochemical impedance spectroscopy (EIS) study of nanostructured Co_3O_4

To get a deeper understanding of the charge transport within the oxide electrocatalyst, EIS analysis was performed. The Bode and Nyquist plots for the $\text{Co}_3\text{O}_4@\text{CMC}$ samples and pristine Co_3O_4 are shown in Figure 6 a,b and Figure 6c, respectively, which gives information about the charge transfer

kinetics. The experimental results for the impedance were simulated by Z-view software to investigate the bulk electrolyte and double layer interfaces. and fitted with equivalent circuit as inset in Figure 5c. The simple Randles circuit was used to represent the interfaces and the circuit fitted equivalent circuit are shown in inset in Figure 6c. elements were S solution resistance R_s represents the bulk solution interface, and charge transfer resistance R_{ct} and constant phase element corresponded to the double layer capacitance interface. The impedance of CPE can be written as $Z_{CPE} = 1/Q(j\omega)^n$, where $j = (-1)^{1/2}$ and n represents the deviation from the ideal behavior, n being 1 for perfect capacitors [53 - 55]. The R_{ct} values from the Nyquist plots for the $Co_3O_4@CMC-1$, $Co_3O_4@CMC-2$ and pristine Co_3O_4 were found 291.3, 131.8 and 1022 Ohms respectively. The lowest value of R_{ct} for the $Co_3O_4@CMC-2$ sample reveals a faster charge transfer kinetics compared to $Co_3O_4@CMC-1$ and pristine Co_3O_4 Figure 6c. Also, the double layer capacitance was calculated from EIS results for the Co_3O_4 , $Co_3O_4@CMC-1$, and $Co_3O_4@CMC-2$ as 0.07, 0.26 and 0.94 mF respectively as given Table 2. A higher value of capacitance indicates the large capability for the transfer of ionic charge between the electrolyte and electrode, corresponding to larger active area. Furthermore, EIS study was also carried on the different $Co_3O_4@PA$ samples and the results are reported in Figure 6 d,e,f. Figure 6 d,e represent the Bode plots obtained from the impedance results: they give information The fitted circuit is also reported as an as inset in Figure 6f. The Nyquist plots are reported in Figure 6f and the Co-25polyacryl exhibited the smallest semicircle, which confirms the faster kinetics and excellent conductivity of the material, compared to the other samples, which further accelerated the charge transport during the OER process. The corresponding R_{ct} and capacitance double layer for Co-25polyacryl and Co-50polyacryl are 82.58 and 129.9 Ohms and 1.56 and 0.94 mF, respectively, as given in Table 2. Once again, Co-25polyacryl exhibits the smallest charge transfer resistance and the largest double layer capacitance in the faradaic regime, confirming the superior electrochemical activity of this specific material, proving how the morphology of the catalyst is responsible for dramatic variation of its functional properties. Unlike CMC, PA addition does not result in improved performance by improving the polymer content, suggesting that the templating mechanism is more complex than a simple stabilization of the growing nanoparticles.

4. Conclusions

In summary, we have produced Co_3O_4 nanostructures in the presence of polyacrylamide and CMC as nucleophilic polymers by wet chemical method. The Co_3O_4 nanostructures were found efficient for OER in 1.0M KOH basic conditions. The prepared materials are physically characterized by XRD, SEM, EDS and HRTEM techniques, highlighting a different role of the templating polyelectrolyte on the nanocrystals morphology. These studies confirmed the short-range nanowire morphology consisting chain of nanoparticles and cubic phase of Co_3O_4 . The short-range nanowires of Co_3O_4 exhibit high surface area along with high density of catalytic centers. The XPS study has shown that the Co-25polyacryl sample is associated to large amount of Co^{3+} ions and the surface oxygen vacancies which dynamically enhanced the oxygen evolution reaction. Robust OER performance were shown both for CMC and Polyacrylamide-templated nanostructures, achieving state-of-the art overpotential and Tafel slope with over 30h stability. The different templating mechanism of the two employed polyelectrolyte resulted in a slight enhancement of the OER performance for the Polyacrylamide-templated samples. The peculiar morphology and the improved oxygen vacancies concentration for this cobalt oxide structures were correlated to the enhanced electrochemical activity. The present study is therefore proving the role of polyelectrolytes-templated growth towards the design of efficient electrocatalysts, highlighting how complex mechanisms might be responsible for unexpected enhancement of the functional properties, as observed with the addition of polyacrylamide. We envision a growing interest in the fine control of structure and surface chemistry of metal oxide electrocatalysts through multifunctional templating agents, towards the enhancement of OER performance. Conclusively, these Co_3O_4 nanostructures obtained with CMC and polyacrylamide are promising electrocatalysts for diverse applications other than OER, such as fuel cells and metal-air batteries.

Acknowledgement

Authors acknowledge the Higher Education of Pakistan for the partial financial support of this research work. A.N thanks Researchers Supporting project (RSP-2021/79) at King Saud University, Riyadh, Saudi Arabia. Authors acknowledge the XPS support from Dr. Kezhen Qi though his financial support under the project “Liaoning Revitalization Talents Program

(XLYC1807238).” China. A.I.M. acknowledges RTI2018-099668-BC22, RyC-2015-17870 and UMA18-FEDERJA-126 projects (Spain). A.G., R.M. and V.M. thanks the E.U. for partial financial support through the Graphene Flagship Core 3 project (Project ID: 881603).

Conflict of Interest

Authors declare no conflict of interest in this research work

5. References

[1] Global energy & CO₂ status report 2019.

<https://www.inderscienceonline.com/doi/abs/10.1504/IJGEI.2002.000965>.

[2] Renewable Energy Now Accounts for a Third of Global Power Capacity, 2019.

<https://www.hydroreview.com/2019/04/03/irena-reports-renewable-energy-now-accounts-for-a-third-of-global-power-capacity/#gref>.

[3] H. Zhang, H. Y. Li, B. Akram, X. Wang, Fabrication of NiFe layered double hydroxide with well-defined laminar superstructure as highly efficient oxygen evolution electrocatalysts. *Nano Res.* 12 (2019) 1327–1331.

[4] R. V. Digraaskar, V. S. Sapner, S. S. Narwade, S. M. Mali, A. V. Ghule and B. R. Sathe, Enhanced electrocatalytic hydrogen generation from water via cobalt-doped Cu₂ZnSnS₄ nanoparticles, *RSC Adv.* 8 (2018) 20341-20346.

[5] V. Maruthapandian, M. Mathankumar, V. Saraswathy, B. Subramanian and S. Muralidharan, Study of the Oxygen Evolution Reaction Catalytic Behavior of Co_xNi_{1-x}Fe₂O₄ in Alkaline Medium, *ACS Appl. Mater. Interfaces.* 9 (2017) 13132 -13141.

[6] J.N. Tiwari, High-performance hydrogen evolution by Ru single atoms and nitrated-Ru nanoparticles implanted on N-doped graphitic sheet. *Adv. Energy Mater.* 9 (2019) 1900931.

[7] Z. Khajehsaeidi, P. Sangpour, A. Gha_arinejad, A novel co-electrodeposited Co/MoSe₂/reduced graphene oxide Nano composite as electro catalyst for hydrogen evolution. *Int. J. Hydrog. Energy.* 44 (2019) 19816–19826.

[8] R. V. Digraaskar, B. B. Mulik, P. S. Walke, A. V. Ghule and B. R. Sathe, Enhanced hydrogen evolution reactions on nanostructured Cu₂ZnSnS₄ (CZTS) electro catalyst, *Appl. Surf. Sci.* 412 (2017) 475-481

- [9] M. Qian, S. Cui, D. Jiang, L. Zhang and P. Du, Highly Efficient and Stable Water- Oxidation Electrocatalysis with a Very Low Overpotential using FeNiP Substitutional- Solid- Solution Nanoplate Arrays, *Adv. Mater.* 29 (2017) 1704075
- [10] Q. He, Highly defective Fe-based oxyhydroxides from electrochemical reconstruction for efficient oxygen evolution catalysis. *ACS Energy Lett.* 3 (2018) 861–868.
- [11] R. Gao, D.P. Yan, Fast formation of single-unit-cell-thick and defect-rich layered double hydroxide nanosheets with highly enhanced oxygen evolution reaction for water splitting. *Nano Res.* 11 (2018) 1883–1894.
- [12] K.L. Liu, The role of active oxide species for electrochemical water oxidation on the surface of 3d-metal phosphides. *Adv. Energy Mater.* 8 (2018) 1703290.
- [13] T. Li, Atomic-scale insights into surface species of electro catalysts in three dimensions. *Nat. Catal.* 1 (2018) 300–305.
- [14] H.Q. Fu, 1D/1D hierarchical nickel sulfide/phosphide nanostructures for electrocatalytic water oxidation. *ACS Energy Lett.* 3 (2018) 2021–2029.
- [15] C. Gu, Synthesis of sub-2 nm iron-doped NiSe₂ nanowires and their surface confined oxidation for oxygen evolution catalysis. *Angew. Chem.* 130 (2018) 4084–4088.
- [16] J. Zhao, Y. Zou, X. Zou, T. Bai, Y. Liu, R. Gao, D. Wang, G.D. Li, Self-template construction of hollow Co₃O₄ microspheres from porous ultrathin nanosheets and efficient noble metal-free water oxidation catalysts, *Nano scale.* 6 (2014) 7255.
- [17] Y. Liang, Y. Li, H. Wang, J. Zhou, J. Wang, T. Regier, H.Dai, Co₃O₄ nanocrystals on graphene as a synergistic catalyst for oxygen reduction reaction, *Nat. Mater.* 10 (2011) 780.
- [18] X. Zou, A.Goswami, T.J. Asefa, J. Am. Efficient noble metal-free (electro) catalysis of water and alcohol oxidations by zinc–cobalt layered double hydroxide, *Chem. Soc.* 135 (2018) 17242.
- [19] B. Jiang, Y. Guo, J. Kim, A. E. Whitten, K. Wood, K. Kani, A. E. Rowan, J. Henzie, Y. Yamauchi, Mesoporous Metallic Iridium Nanosheets, *J. Am. Chem. Soc.* 140 (2018) 12434.
- [20] C. Li, M. Iqbal, B. Jiang, Z. Wang, J. Kim, A. K. Nanjundan, A. E. Whitten, K. Wood, Y. Yamauchi, Pore-tuning to boost the electrocatalytic activity of polymeric micelle-templated mesoporous Pd nanoparticles, *Chem. Sci.*, 10 (2019) 4054.

- [21] C. Li, H. Tan, J. Lin, X. Luo, S. Wang, J. You, Y.-M. Kang, Y. Bando, Y. Yamauchi, J. Kim, Emerging Pt-based electrocatalysts with highly open nanoarchitectures for boosting oxygen reduction reaction (Review), *Nano Today*. 21 (2018) 91.
- [22] C. Li, M. Iqbal, J. Lin, X. Luo, B. Jiang, V. Malgras, K. C-W. Wu, J. Kim, Y. Yamauchi, Electrochemical Deposition: An Advanced Approach for Templated Synthesis of Nanoporous Metal Architectures, *Acc. Chem. Res.* 51 (2018) 1764.
- [23] H. Tueysuez, Y.J. Hwang, S.B. Khan, A.M. Asiri, P. Yang, A mini review of NiFe-based materials as highly active oxygen evolution reaction electrocatalysts, *Nano Res.* 6 (2013) 47.
- [24] J.A. Koza, Z.He, A.S.Miller, S.Switzer, Electrodeposition of Crystalline Co_3O_4 : A Catalyst for the Oxygen Evolution Reaction, *J. A. Chem. Mater.* 24 (2012) 3567.
- [25] D. Klemm, B. Heublein, H. P. Fink, A. Bohn, *Angew. Chemie, Cellulose: Fascinating Biopolymer and Sustainable Raw Material*, - Int. Ed. 44 (2005) 3358.
- [26] Y. M. Chen ,L. Sun, A. Yang, Biomedical applications of hydrogels: A review of patents and commercial products, *European Polymer Journal*. 94 (2017) 501-16.
- [27] F. F. Barbosa, A. P. F. Paulista, M. A. M. Torres, T. Pinheiro Braga, Synthesis of the Fe–Co alloy from hybrid spheres using carboxymethylcellulose as template and its application in catalysis, *Mater. Chem. Phys.* 242 (2020) 122550.
- [28] D. Klemm, B. Heublein, H. P. Fink, A. Bohn, New approaches to advanced polymers by selective cellulose functionalization, *Acta Polymerica*. 48 (1997) 277-95
- [29] V. Pace, W. Holzer, B. Olofsson, Increasing the Reactivity of Amides towards Organometallic Reagents: An Overview, *advanced synthesis catalysis*. 356 (2014) 3697.
- [30] T. Jayaramudu, H. Ko, H. Kim, J. Kim and J. Kim, Swelling Behavior of Polyacrylamide–Cellulose Nanocrystal Hydrogels: Swelling Kinetics, Temperature, and pH Effects, *Materials (Basel)*. 12 (2019) 2080-98.
- [31] B. Bolto, J. Gregory, Organic polyelectrolytes in water treatment, *Water Res.* 41 (2007) 2301-23.

- [32] H. Zheng, J. Ma, F. Ji, X. Tang, W. Chen, J. Zhu, Y. Liao, M. Tan, Applications of Inorganic Coagulant for Typical Organic Contaminants Removal from Water: A Review, *Asian J. Chem.* 25 (2013) 7071-96.
- [33] M. Chen, Y. Jiang, P. Mei, Y. Zhang, X. Zheng, W. Xiao, Q. You, X. Yan, H. Tang, Polyacrylamide Microspheres-Derived Fe₃C@N-doped Carbon Nanospheres as Efficient Catalyst for Oxygen Reduction Reaction, *Polymers*. 11 (2019) 767-95.
- [34] M. C. Biesinger, B. P. Payne, P. Grosvenor, W. M. Lau, A. R. Gerson, Resolving surface chemical states in XPS analysis of first row transition metals, oxides and hydroxides: Cr, Mn, Fe, Co and Ni, *Applied Surface Science*. 257 (2011) 2717-32.
- [35] K. Föttinger, G. Rupprechter, In Situ Spectroscopy of Complex Surface Reactions on Supported Pd–Zn, Pd–Ga, and Pd (Pt)–Cu Nanoparticles, *Acc. Chem. Res.* 47 (2014) 3031-43.
- [36] A. P. Grosvenor, S. D. Wik, R. G. Cavell, A. Mar, Examination of the bonding in binary transition-metal monophosphides MP (M = Cr, Mn, Fe, Co) by X-ray photoelectron spectroscopy, *Inorg. Chem.* 44 (2005) 8988-98.
- [37] M. K. Keshmarzi, A. A. Daryakenari, H. Omidvar, M. J. Bakht, Z. Ahmadi, J.-J. Delaunay, R. Badrnezhad, Pulsed electrophoretic deposition of nanographitic flake-nanostructured Co₃O₄ layers for efficient lithium-ion-battery anode, *J. of Alloys and Comp.* 805 (2019) 924-46.
- [38] K. Wang, Y. Cao, J. Hu, Y. Li, J. Xie, D. Jia, Solvent-Free Chemical Approach to Synthesize Various Morphological Co₃O₄ for CO Oxidation, *ACS Appl. Mater. Interfaces*. 9 (2017) 16128.
- [39] C. Dong, Z. Qu, Y. Qin, Q. Fu, H. Sun, X. Duan, Revealing the Highly Catalytic Performance of Spinel CoMn₂O₄ for Toluene Oxidation: Involvement and Replenishment of Oxygen Species Using In Situ Designed-TP Techniques, *ACS Catal.* 9 (2019) 6698.
- [40] M. Nischk, P. Mazierski, Z. Wei, K. Siuzdak, N. A. Amoin, K. Ewa, Low-power microwave-induced fabrication of functionalised few-layer black phosphorus electrodes: A novel route towards Haemophilus Influenzae pathogen biosensing devices, *Applied Surface Science*. 387 (2016) 102-24.

- [41]. M.jing,W.Zhurui ,S.Xiaodong ,Z.Fanpeng ,D.Huijun ,Y.Huiming, Metal–Organic Framework-Derived Nanoporous Metal Oxides toward Supercapacitor Applications: Progress and Prospects, *Journal of Hazardous Materials*. 371 (2019) 361-83.
- [42] J.Zhong ,Y.Zenga ,M.Zhang ,W.Fenga ,D.Xiao , Ultrathin Graphene Layers Encapsulating Nickel Nanoparticles Derived Metal–Organic Frameworks for Highly Efficient Electrocatalytic Hydrogen and Oxygen Evolution Reactions, *Chemical Engineering Journal*. 397 (2020) 125375.
- [43] V. Iablokov, R. Barbosa, G. Pollefey, I. Van Driessche, S. Chenakin and N. Kruse, Catalytic CO oxidation over well-defined cobalt oxide nanoparticles: size-reactivity correlation, *ACS Catal.* 5 (2015) 5718.
- [44] D. Gu, C.J. Jia, C. Weidenthaler, H-J. Bongard, B. Spliethoff, W. Schmidt, and F. Schüth, Highly Ordered Mesoporous Cobalt-Containing Oxides: Structure, Catalytic Properties, and Active Sites in Oxidation of Carbon Monoxide, *J. Am. Chem. Soc.* 137 (2015) 11407.
- [45] T. Hua, Y. Wanga, L. Zhanga, T. Tanga, H.Xiaoa, W. Chena, M. Zhaoa, J. Jiaa, H. Zhub, Facile synthesis of PdO-doped Co₃O₄ nanoparticles as an efficient bifunctional oxygen electrocatalyst, *App. Catalysis B: Environ.* 243 (2019) 175–182.
- [46] L. Zhang, C. Lu, F. Ye, Z. Wu, Y. Wang, L. Jiang, L. Zhang, C. Cheng, Z. Sun, L. Hu, Vacancies boosting strategy enabling enhanced oxygen evolution activity in a library of novel amorphous selenite electrocatalysts, *App. Catalysis B: Environ.* 284 (2021) 119758.
- [47] D. Chen, J. Zhu, X. Mu, R. Cheng, W. Li, S. Liu, Z. Pu, C. Lin, S. Mu, Nitrogen-Doped carbon coupled FeNi₃ intermetallic compound as advanced bifunctional electrocatalyst for OER, ORR and zn-air batteries, *App. Catalysis B: Environ.* 268 (2020) 118729.
- [48] S. Xu, M. Wang, G. Saranya, N. Chen, L. Zhang, Y. He, L. Wu, Y. Gong, Z. Yao, G. Wang, Z. Wang, S. Zhao, H. Tang, M. Chen, H. Gou, Pressure-driven catalyst synthesis of Co-doped Fe₃C@Carbon nano-onions for efficient oxygen evolution reaction, *App. Catalysis B: Environ.* 268 (2020) 118385.
- [49] K.A. Stoerzinger, L. Qiao, M.D. Biegalski, Y. Shao-Horn, Orientation-Dependent Oxygen Evolution Activities of Rutile IrO₂ and RuO₂, *J. Phys. Chem. Lett.* 5 (2014) 1641.

- [50] H. S. Jeon, M. S. Jee, H. Kim, S. J. Ahn, Y. J. Hwang, B. K. Min, Simple Chemical Solution Deposition of Co_3O_4 Thin Film Electrocatalyst for Oxygen Evolution Reaction, ACS Appl. Mater. Interfaces. 44 (2015) 24550–24555
- [51] N.H. Chou, P. N. Ross, A. T. Bell, T. D. Tilley, Comparison of cobalt-based nanoparticles as electrocatalysts for water oxidation., ChemSusChem. 4 (2011) 1566-1569
- [52] H. Tüysüz, Y.J. Hwang, S. B. Khan, A. M. Asiri & P. Yang, Mesoporous Co_3O_4 as an electrocatalyst for water oxidation, Nano Research. 6 (2013) 47–54.
- [53] N.-T. Suen, S.-F. Hung, Q. Quan, N. Zhang, Y.-J. Xu, H. M. Chen. Electrocatalysis for the oxygen evolution reaction: recent development and future perspectives, Chem. Soc. Rev., 46 (2017) 337.
- [54] A. Rebekah, S. Anantharaj, C. Viswanthan, N. Ponpandian, Zn-substituted MnCo_2O_4 nanostructure anchored over rGO for boosting the electrocatalytic performance towards methanol oxidation and oxygen evolution reaction (OER), I. J. hydrogen energy. 45 (2020) 14713-14727.
- [55] K. Lemoine, J. Lhoste, A. Hémon-Ribaud, N. Heidary, V. Maisonneuve, A. Guet, N. Kornienko, Investigation of Amorphous Mixed-Metal (Oxy)Fluorides as a New Class of Water Oxidation Electrocatalysts, ChemRxiv, (2019) DOI: [10.26434/chemrxiv.9456158](https://doi.org/10.26434/chemrxiv.9456158)

Figure Captions

Figure 1. Distinctive SEM images, **1a** pure Co_3O_4 , **1b**. Co_3O_4 @CMC- 1 (S1), **1c**. Co_3O_4 @CMC-2 (S2), **d**. Co-25polyacryl; **e**Co-50polyacryl; (d)

Figure 2. Powder XRD diffraction patterns, **1a** pure Co_3O_4 , **1b.** $\text{Co}_3\text{O}_4@\text{CMC}-1$ (S1), **1c.** $\text{Co}_3\text{O}_4@\text{CMC}-2$ (S2) , **1d.** Co-25polyacryl, **1e.** Co-50polyacryl

Figure 3. Low magnification TEM micrographs of pristine Co_3O_4 (a) , Co-25polyacryl (d) and $\text{Co}_3\text{O}_4@\text{CMC}$ (g) sample; high magnification TEM micrograph of pristine Co_3O_4 (b), Co-25polyacryl (e) and $\text{Co}_3\text{O}_4@\text{CMC}$ (h) sample ; HR-TEM with FFT of pristine Co_3O_4 (c), Co-25polyacryl (f) and $\text{Co}_3\text{O}_4@\text{CMC}$ (i) sample.

Figure 4. (a) Co $2p$, (b) Co Auger and c) O $1s$ XPS spectra of Co-25polyacryl and $\text{Co}_3\text{O}_4@\text{CMC}-2$

Figure 5. a. Linear sweep voltammetry curves for pristine Co_3O_4 , $\text{Co}_3\text{O}_4@\text{CMC}-1$ (S1), $\text{Co}_3\text{O}_4@\text{CMC}-2$ (S2) at scan rate 1 mV/s in aqueous solution of 1.0M KOH, **b.** The Tafel plotting from LSV curves, **c.** Durability of $\text{Co}_3\text{O}_4@\text{CMC}-2$ (S2), through chronopotentiometry experiment at a fixed 15 mAcm^{-2} for 30 h, **d.** LSV curves before and after the durability test, **e.** Linear sweep voltammetry Co-25polyacryl, Co-50polyacryl, 20% RuO_2/C at scan rate 1 mV/s in 1.0M KOH, **f.** The Tafel plots from LSV curves, **g.** Durability of Co-25polyacryl through chronopotentiometry experiment at a constant 10 mAcm^{-2} for 30 h, **h.** Stability of Co-25polyacryl.

Figure 6. Electrochemical impedance spectra of pure Co_3O_4 , $\text{Co}_3\text{O}_4@\text{CMC}-1$ (S1), $\text{Co}_3\text{O}_4@\text{CMC}-2$ (S2) in 1.0M KOH at 100 kHz to 0.1Hz with sinusoidal potential of 10 mV and OER onset potential, the Bode plots (**a,b**) and **c.** Nyquist Plots, EIS results for Co_3O_4 nanostructures Co-25polyacryl, Co-50polyacryl, using a in 1.0M KOH at 100 kHz to 0.1Hz with sinusoidal potential of 10 mV and OER onset potential in 1.0M KOH, the Bode plots (**d,e**), and **f.** Nyquist Plots.

Figure 1

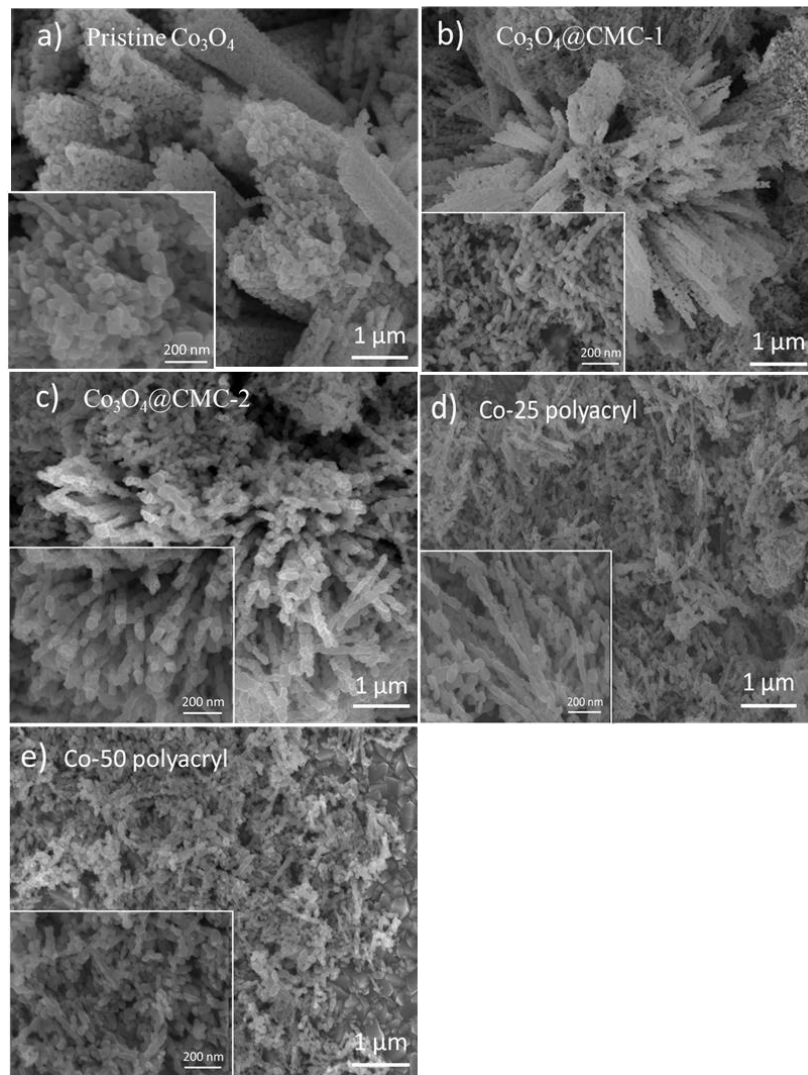


Figure 2



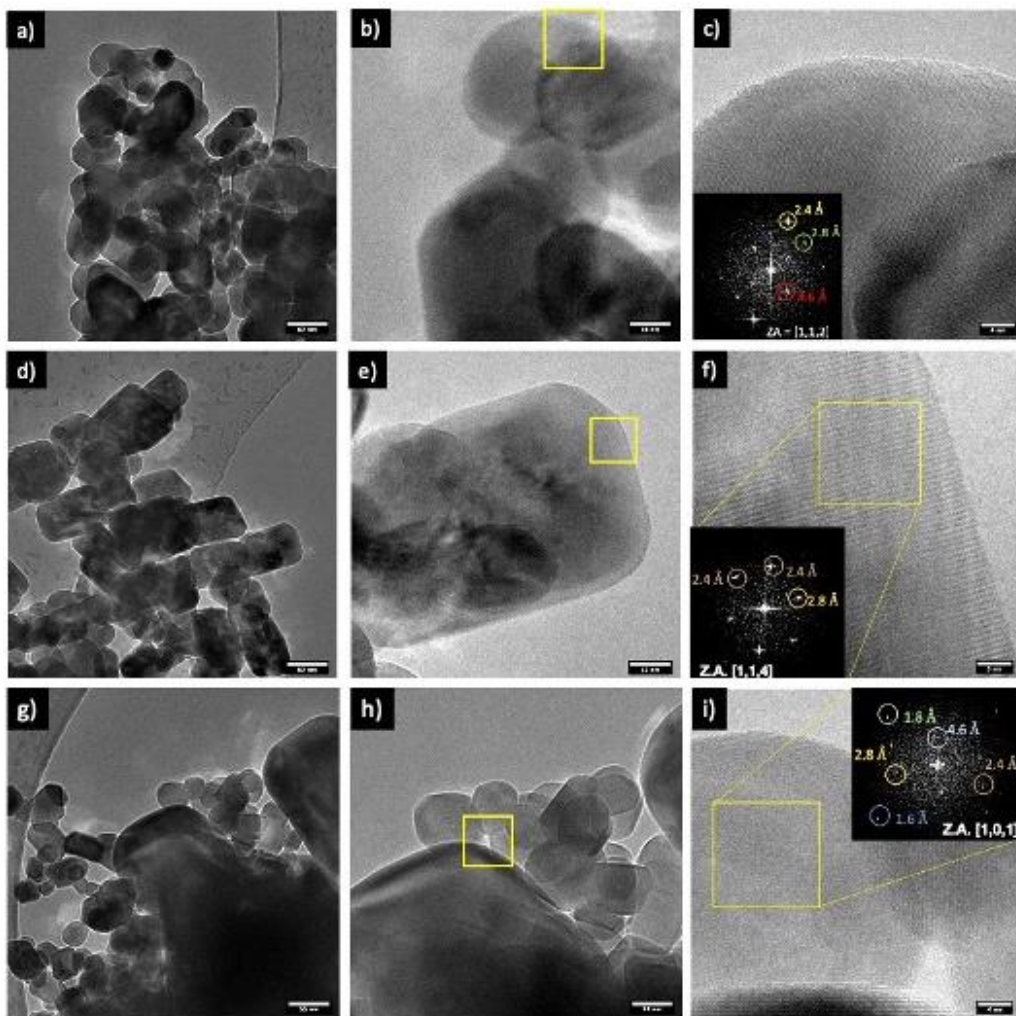


Figure 4

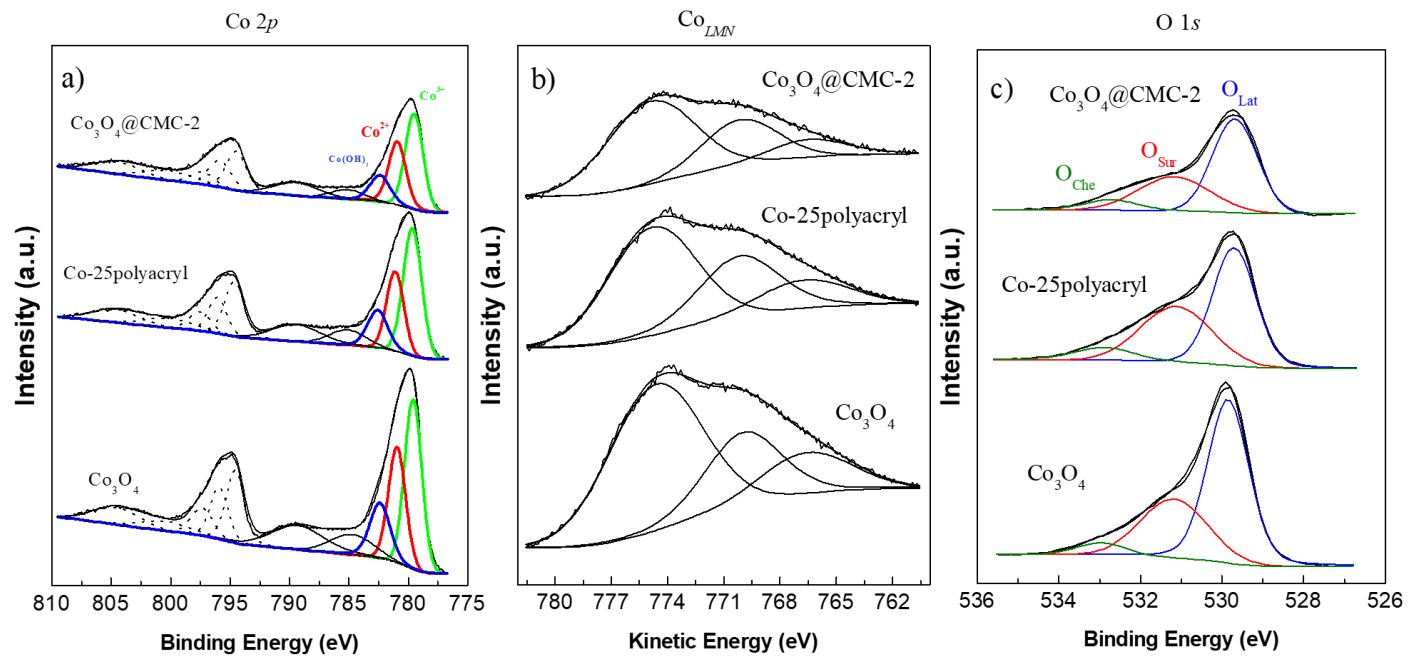


Figure 5

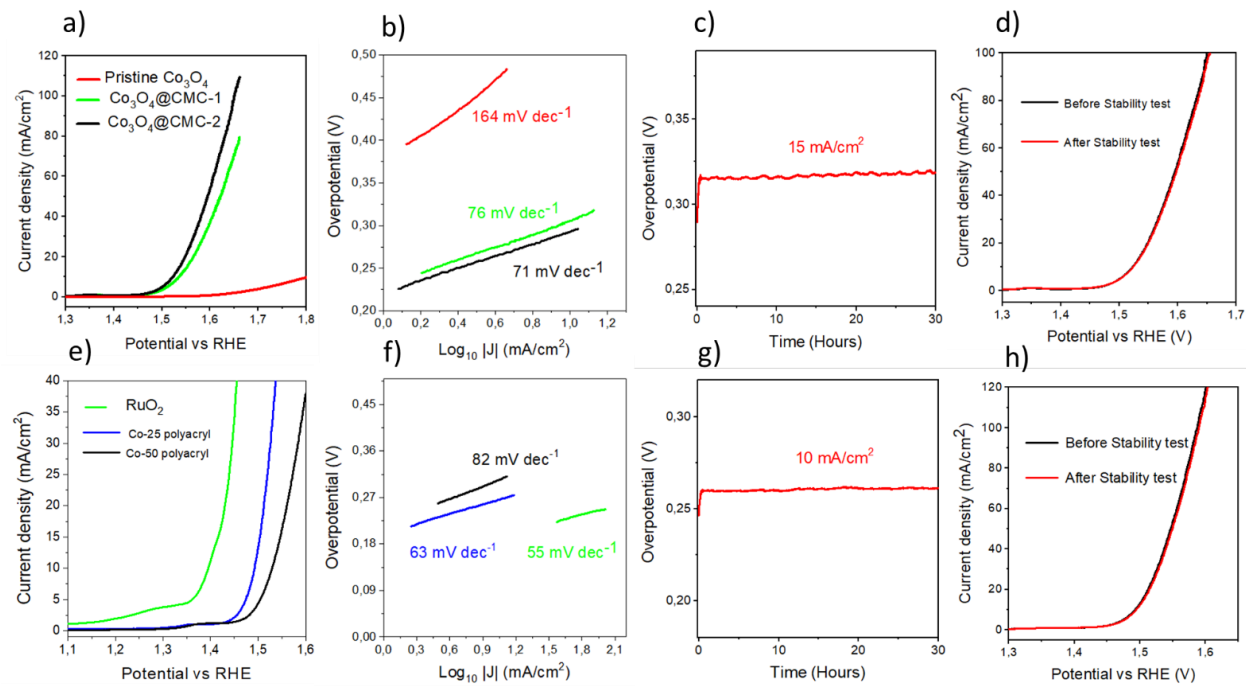


Figure 6

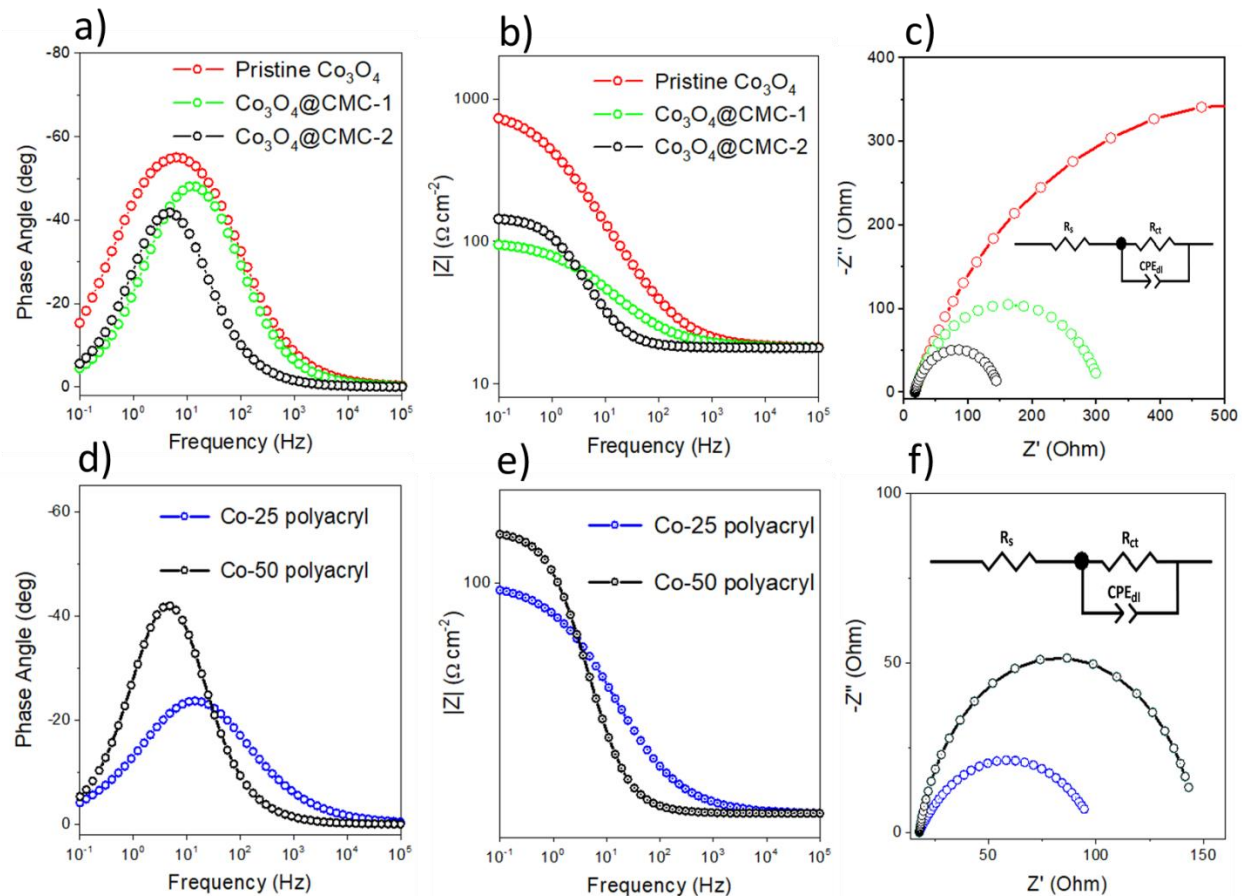


Table 1. XPS decomposition result of the studied samples

	Co 2 <i>p</i>		Co _{LMN}	α'	O 1 <i>s</i>		
	BE (eV)	%	KE (eV)	(eV)	BE (eV)	%	O _{Surf} /O _{La} /
Co ₃ O ₄	779.6	34.3	774.6	1554.2	529.9	61.7	0.53
	780.9	23.6	770.0	1550.9	531.2	32.9	
	782.4	14.3	766.6	1549.0	533.0	5.4	
Co- 25polyacryl	779.7	38.0	774.8	1554.5	529.7	52.1	0.75
	781.1	22.1	770.2	1551.3	531.1	38.9	
	782.6	13.4	766.7	1549.3	532.9	9.0	
Co ₃ O ₄ @CMC- 2	779.5	35.3	774.9	1554.4	529.7	57.9	0.58
	780.9	24.7	770.2	1551.1	531.2	33.7	
	782.4	12.1	766.5	1548.9	532.7	8.4	

Table 2: Summary of unique features of Co₃O₄ grown with CMC and Polyacryl.

Catalyst	Calculated from LSV	Calculated from EIS	
		Tafel Slope	Charge Transfer Resistance
		Double Layer Capacitance	
	<i>B</i>	<i>R_{ct}</i>	<i>CPE_{dl}</i>
	<i>mV/dec</i>	Ω	<i>mF</i>
Pristine Co ₃ O ₄	164	1022	0.07
Co ₃ O ₄ @CMC-1	76	291.3	0.26
Co ₃ O ₄ @CMC-2	71	131.8	0.94
Co-25polyacryl	63	82.58	1.56
Co-50polyacryl	82	129.9	0.94

Supplementary data

Nanostructured Co₃O₄ electrocatalyst for OER: the role of organic polyelectrolytes as soft templates

Adeel Liaquat Bhatti^a, Aneela Tahira^c, Alessandro Gradone^{e,g}, Raffaello Mazzaro^{e*}, Vittorio Morandi^e, Umair aftab^d, Ayman Nafadyⁱ, Kezhen Qi^h, Antonia Infantes-Molina^j, Alberto Vomiero^{f,g}, Zafar Hussain Ibupoto^{b*}

^aInstitute of Physics University of Sindh Jamshoro, 76080, Sindh Pakistan

^bDr. M.A Kazi Institute of Chemistry University of Sindh Jamshoro, 76080, Sindh Pakistan

^cDepartment of Science and Technology, Campus Norrkoping, Linkoping University, SE-60174 Norrkoping, Sweden

^dMehran University of Engineering and Technology, 7680 Jamshoro, Sindh Pakistan

^eInstitute for Microelectronics and Microsystems, Italian National Research Council, Section of Bologna, Via Piero Gobetti 101, 40129, Bologna, Italy

^fDivision of Material Science, Department of Engineering Sciences and Mathematics, Luleå University of Technology, 97187 Luleå, Sweden

^gDepartment of Molecular Sciences and Nanosystems, Ca' Foscari University of Venice, Via Torino 155, 30172 Venezia Mestre, Italy

^hInstitute of Catalysis for Energy and Environment, College of Chemistry and Chemical Engineering, Shenyang Normal University, Shenyang 110034, China

ⁱDepartment of Chemistry, College of Science, King Saud University, Riyadh 11451, Saudi Arabia

^jDepartment of Inorganic Chemistry, Crystallography and Mineralogy. (Unidad Asociada al ICP-CSIC), Faculty of Sciences, University of Malaga, Campus de Teatinos, 29071 Malaga, Spain.

Corresponding authors: Zafar Hussian Ibupoto, PhD*, Raffaello Mazzaro, PhD*

Email address: zaffar.ibhupoto@usindh.edu.pk, mazzaro@bo.imm.cnr.it

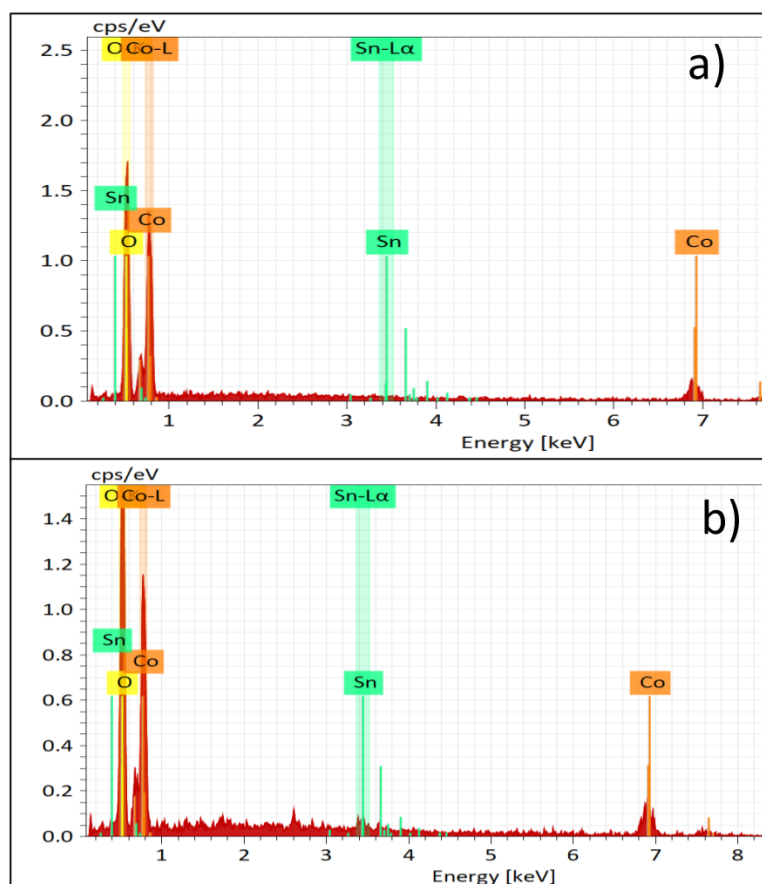


Figure S1. a. EDS spectrum for Co₃O₄@CMC-2, b. EDS spectrum for Co-25 polyacryl sample

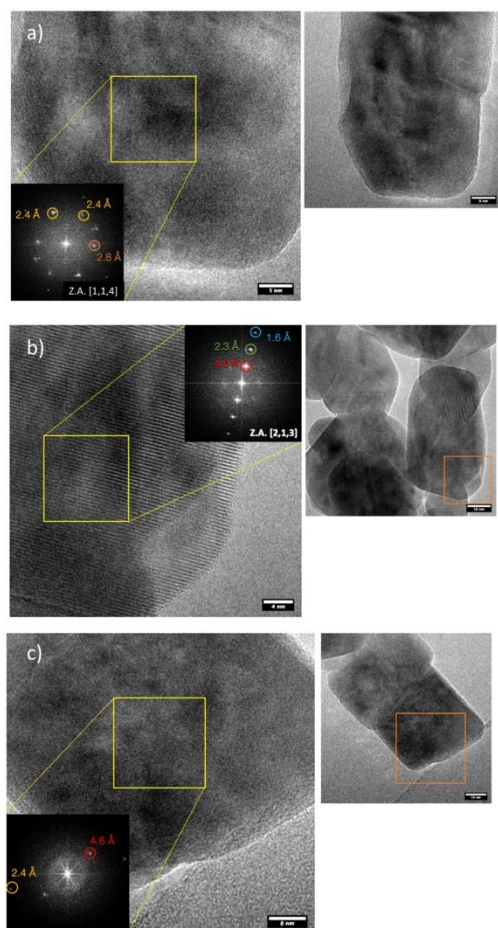


Figure S2. HR-TEM micrographs of Co-50 polyacryl sample exhibiting either spinel $\text{Co}_3\text{O}_4[1,1,4]$ (a) or reflection perpendicular to the squared edge of the nanocrystals, with d-spacing 0.46 nm, corresponding to $[1,1,1]$ planes.

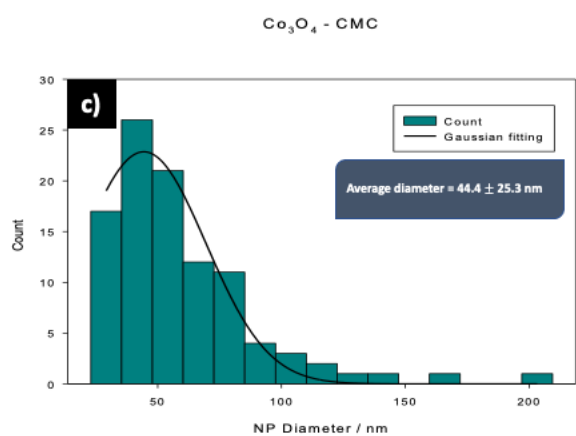
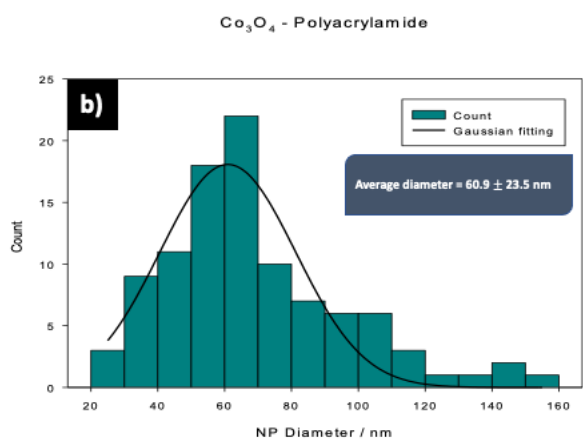
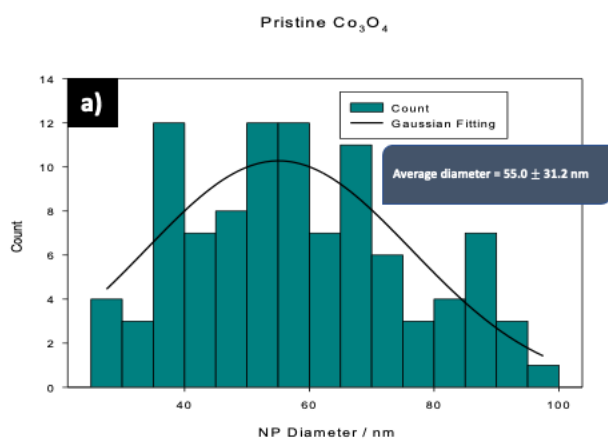


Figure S3. Size distribution of pristine Co_3O_4 (a) Co -25polyacryl (b) and $\text{Co}_3\text{O}_4@\text{CMC}$ (c) sample, taking into account 100 nanoparticles. All the histogram fitting has been done with a 3 parameter gaussian equation, $y = a e^{[-0.5*(x-x_0)^2/2]}$.

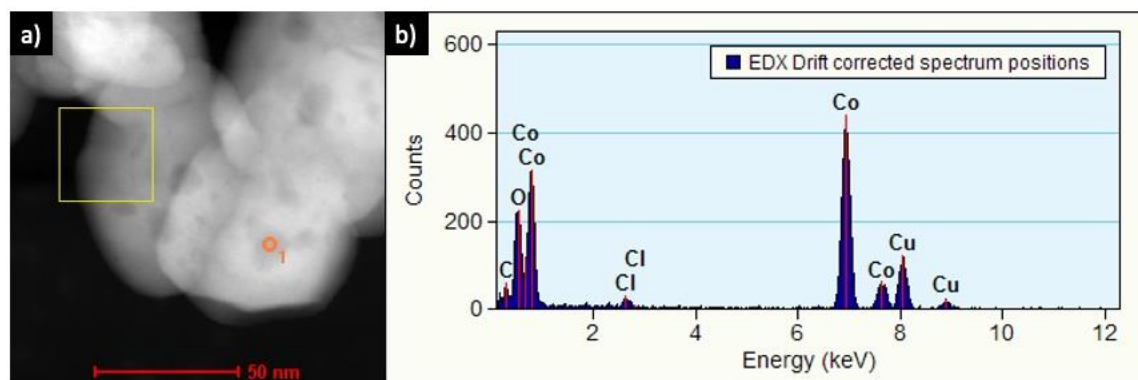


Figure S4 EDS position analysis of the spot 1 highlighted in figure a) of Co-25 polyacryl sample. **a.** STEM-HAADF micrograph of Co -25 polyacryl sample **b.** EDS position analysis of the spot 1 highlighted in figure a) of Co-25 polyacryl sample

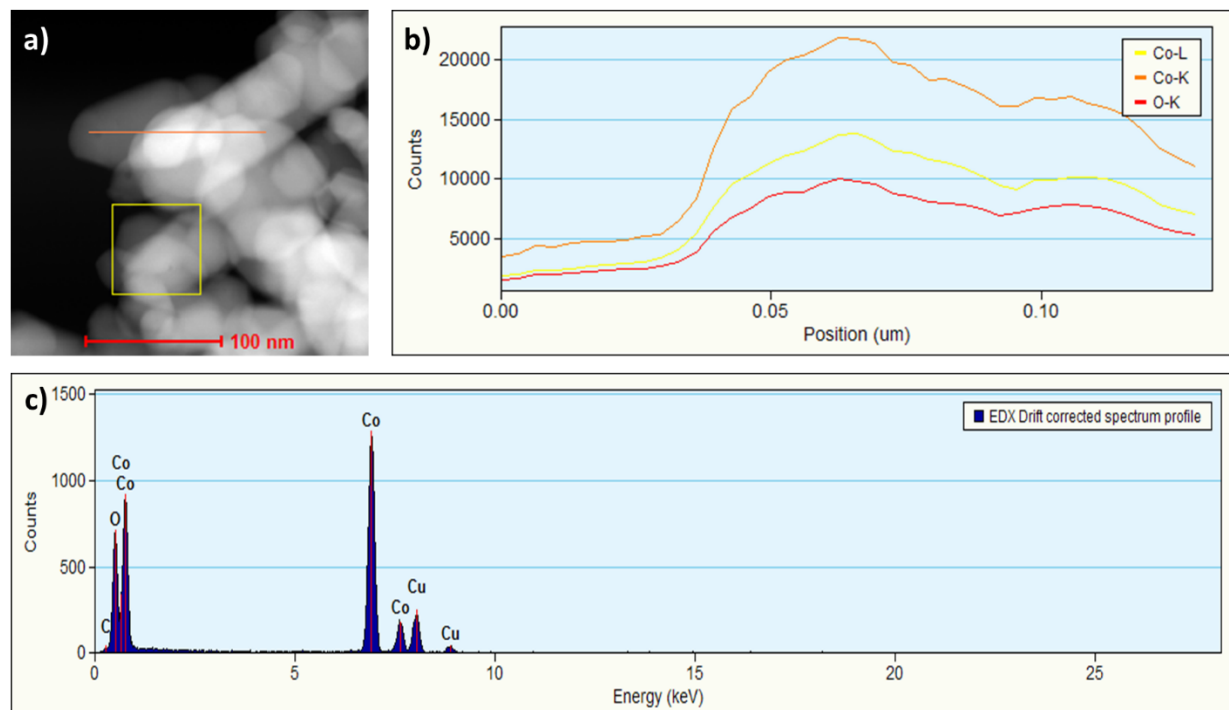


Figure S5. a) STEM-HAADF micrograph of $\text{Co}_3\text{O}_4@\text{CMC2}$ sample; b) EDS profile reconstruction of the orange line highlighted in figure a); c) EDS position analysis of the first point recorded in the scan.

Table S1: The comparison of OER activity of presented Co_3O_4 -25 polyacryl electrocatalyst with recently reported works in 1.0M KOH

Catalyst	Overpotential (η) (mV @10mA cm ⁻²)	Tafel Slope mVdec ⁻¹	References
Co5.47N NP@N-PC	248	72	1
$\text{Co}_3\text{O}_4@\text{MoS}_2$	269	58	2
CoP	370	100	3
$\text{Co}_x\text{Ni}_{1-x}\text{S}_2$	320	52	4
CoB	580	42	5
NiCo_2O_4	396	110	6
$\text{Ni}_{0.6}\text{Co}_{1.4}\text{P}$ nanocages	300	80	7
Co-Ni-B@NF	490	93	8
Cobalt/Carbon nanocomposite	296	50.9	9
NiCoO_4	350	43	10
$\text{NaCo}(\text{PO}_3)_3$	340	51	11
$\text{NiCoO}_4\text{N/NF}$	290	65	12
Cobalt-cobalt oxide/ n-doped carbon hybrids	260	77	13

Spinel NiCo ₂ O ₄ nanoflowers on grapheme	383	137	14
3 D CoNi skeleton	262	58	15
CoCrRu LDHs	290	56	16
BC/Co ₃ O ₄	310	52	17
Co ₃ O ₄ -25 polyacryl	260	63	This work

- [1] Y. Jin, S. Huang, X. Yue, H. Du, P.K. S.Mo ,ACS Catal2018, 8 , 2359.
- [2] J. Liu, J. Wang, B. Zhang, Y. Ruan, H. Wan, X. Ji, K. Xu, D. Zha, L. Miao, J. Mater. Chem. A. 2018, 6, 2067.
- [3] Y.-R. Hong, S. Mhin, K.-M. Kim, W.S. Han, H. Choi, G. Ali, K.Y. Chung, H.J. Lee, S.-I. Moon, S. Dutta, S. Sun, Y.-G. Jung, T. Song, H. Han, J. Mater. Chem. A. 2019,7, 3592.
- [4] B. Qiu, L. Cai, Y. Wang, Z. Lin, Y. Zuo, M. Wang, Y. Chai, Adv. Funct. Mater. 2018,28, 1707.
- [5] T. Haq , S. A. Mansour, A. Munir, Y. Haik, Advanced Functional Materials. , 2020 ,24,152.
- [6] Y. L. Tong, B. Q. Chi, D. L. Qi, X. Y. Liu, Sci. Adv. Mater. 2019 ,6 ,11.
- [7] D. Y. Lei, X. D. Li, M. K. Seo, M. S. Khil, H. Y. Kim, B. S. Kim ,Polymer. 2017,132.
- [8] B. Qiu, L. Cai, Y. Wang, Z. Lin, Y. Zuo, M. Wang, Y ,Adv Funct Mater.2018, 28 , 1708.
- [9] M. Biegun, X. Chen, Chem ElectroChem.2018 ,5 , , 2681.
- [10]C. Broicher, F. Zeng, J. Artz, H. Hartmann, A. Besmehn, S. Palkovits, j.ChemCatChem. 2019,11 , , 412.
- [11] Y. Wang, B. Zhang, W. Pan, H. Ma, J. ChemSusChem.2017, 10 , 4170.
- [12] R. Gond, D.K. Singh, M. Eswaramoorthy, P. j. Chemie.2019, 58 , 8330.
- [13]N. Xu, G. Cao, Z. Chen, Q. Kang, H. Dai, P. Wang.J.Mater.Chem,A.2017, 5 , 12379.
- [14] Z. Li, B. Li, J. Chen, Q. Pang, P. Int J Hydrogen Energy.2019, 44 , 16120.
- [15] H. Yuan ,S.Wei ,B. tang,Z. Ma, J. chemistry sustainable energy.2020,24 .
- [16] C. Dong ,Xilin Zhang Jie Xu ,J. Sheng . J nano micro small.2020,31 ,16120.
- [17]L. Zou ,Q. Xu , Chem,Asian journal. 2020, 27

1
2
3
4
5
6
7
8
9
10
11
12
13
14
15
16
17
18
19
20
21
22
23
24
25
26
27
28
29
30
31
32
33
34
35
36
37
38
39
40
41
42
43
44
45
46
47
48
49
50
51
52
53
54
55
56
57
58
59
60
61
62
63
64
65